PNAS
www.pnas.org

Supplementary Information for

Femtosecond X-Ray diffraction; Molecular movies of nonadiabatic dynamics

Kochise Bennett, Markus Kowalewski, Jeremy R. Rouxel, Shaul Mukamel

Shaul Mukamel
E-mail: smukamkel@uci.edu

This PDF file includes:

Supporting Information Text

A. Electronic Structure Calculations and Nonadiabatic Wavepacket Dynamics. The electronic structure of NaF was calculated with the program package Molpro (1) at the CAS(8/9)/MRCI/aug-cc-pVTZ level of theory. A Douglas-Kroll-Hess 10th order correction has been used (2, 3) to account for relativistic effects caused by the core electrons. All densities were evaluated from the state specific charge density matrices $P^{(ij)}$, expanded in the atomic orbital basis functions $\phi_r(\mathbf{r})$:

$$\hat{\sigma}_{ij}(\mathbf{q};R) = \int \mathrm{d}\mathbf{r} e^{-i\mathbf{q}\cdot\mathbf{r}} \sum_{rs} P_{rs}^{(ij)}(R)\phi_r^*(\mathbf{r};R)\phi_s(\mathbf{r};R). \quad [S1]$$

Here, $P_{rs}^{(ij)}$ are the matrix elements of the electronic charge-density matrix connecting states i and j in the basis of the atomic orbitals (indices r and s).

Both the transition dipole and the integrated transition density $\int dr|\sigma_{ge}|$ shown in Fig. S3 peak at the avoided crossing point. The relevant electronic density operators matrix elements $\sigma_{ik}^*(\mathbf{q};R)\sigma_{kj}(\mathbf{q};R)$ for the S_1 signal are displayed in Fig. S4. For clarity, only the projection along the direction of molecular axis obtained by integrating over the perpendicular directions is shown. The diagonal density σ_{ee}^2 (Fig. S4 (a)) is clearly dominated by contributions from the core electrons and the stripe pattern reflects the bond length in reciprocal space (see Eq. 15). The transition density σ_{ge}^2 (Fig. S4 (b)) mainly contains contributions from the valence orbitals that are involved in the $|e\rangle \leftrightarrow |g\rangle$ transition. Its magnitude is about 4 orders weaker than the diagonal matrix element (Fig. S4(a)). However, it peaks at the avoided crossing, making it most suitable for the detection of inelastic contributions. The mixed matrix element $\sigma_{ee}^\dagger\sigma_{eg}$ (Fig. S4(c)) is a product of the nuclear densities and the transition densities and its magnitude is about 2 orders weaker than the diagonal matrix element. The transition charge density may thus be measurable through this term in which it is amplified by the diagonal charge density.

Nuclear wave packet dynamics simulations were carried out on a numerical grid in the nuclear coordinate R. This is an exact quantum mechanical calculation of the joint nuclear-electronic dynamics. The Hamiltonian, which describes the coupled electronic and vibrational degrees of freedom, is given by

$$\hat{H} = \begin{pmatrix} \hat{T} + V_g(R) & -E_{pu}(t)\mu_{eg}(R) + \hat{K}_{ge} \\ -E_{pu}(t)\mu_{ge}(R) - \hat{K}_{eg} & \hat{T} + V_e(R), \end{pmatrix} \quad [S2]$$

where

$$\hat{T} = -\frac{1}{2m}\frac{\partial^2}{\partial R^2} \quad [S3]$$

is the kinetic energy operator of the nuclei, m the reduced mass of the nuclei, and

$$\hat{K}_{ge} = \frac{1}{2m}\left(2f_{ge}\frac{\partial}{\partial R} + \frac{\partial}{\partial R}f_{ge}\right) \quad [S4]$$

approximates the non-adiabatic couplings (4, 5). The nuclear wave function $\chi(R,t)$ is obtained by propagating the vibrational ground state of the $X^1\Sigma$ state with a Chebychev scheme (6) using the Hamiltonian Eq. S2.

We assume a Gaussian pump-pulse envelope

$$E_{pu}(t) = E_0\cos(\omega t)\exp(-2\ln(2)t^2/w^2) \quad [S5]$$

where w is the full width at half maximum of the intensity profile E_{pu}^2. The probe pulse is not explicitly included in the propagation but is treated pertubatively and included in the final signal calculation.

Interpretation of S_1

The internuclear distances and thus the shape of the nuclear wave packet can be extracted directly from the diffraction pattern. Figure 7(c) can be qualitatively explained by the following model where the charge density of a diatomic molecule is taken as:

$$\hat{\sigma}(r;R) = \delta(r) + \delta(r-R) \quad [S6]$$

with R the internuclear distance and r is the electronic coordinate The density operator is then given by:

$$\hat{\sigma}(q;R) = \int \mathrm{d}r\, e^{-iqr}\sigma(r) = e^{iqR} + 1 \quad [S7]$$

The S_1 signal is now proportional to:

$$\hat{\sigma}^\dagger(q;R)\hat{\sigma}(q;R) = 2(1+\cos(qR)) \quad [S8]$$

whose inverse Fourier transform peaks at the internuclear distance.

$$\int \mathrm{d}q\, e^{iqr}\hat{\sigma}^\dagger(q)\hat{\sigma}(q) = \delta(r) + \frac{1}{2}\left(\delta(r-R) + \delta(r+R)\right) \quad [S9]$$

Note that for a diatomic molecule the phases of $\sigma(\mathbf{q})$ are not needed for the approximate reconstruction of the real space picture, since we are only looking at a single distance between the two centers. This is of course no longer the case for oriented polyatomic molecules, where the phases are needed to determine the position of the atoms in 3-dimensional space.

Introducing a Gaussian nuclear wavefunction

$$\chi(R) = \left(\frac{\pi}{2\alpha}\right)^{\frac{1}{4}} e^{-\alpha(R-R_1)^2}, \tag{S10}$$

leads to

$$\int \mathrm{d}q\, e^{iqr} \langle\chi|\hat{\sigma}^\dagger(q)\hat{\sigma}(q)|\chi\rangle = \frac{\pi}{2\sqrt{\alpha}}\left(e^{-2\alpha(r+R_1)} + e^{-2\alpha(r-R_1)}\right) + \frac{\pi^2}{\alpha\sqrt{2}}\delta(r). \tag{S11}$$

The spread of the nuclear wave packet translates into a spread in r. If the electronic charge density has a significant width, then that spread becomes a convolution of the width of the nuclear wave packet and the width of the electronic charge density. Moreover, the temporal profile of the probe pulse causes a convolution in the time domain (Eq. 12), thus requiring pulses that are shorter than the nuclear motion in order to observe it.

Light Scattering in the Minimal Coupling Picture

For convenience, we define the interaction current

$$\hat{\mathbf{J}}_{\mathrm{int}}(\mathbf{r}) = \hat{\mathbf{j}}(\mathbf{r}) - \frac{1}{2}\hat{\sigma}(\mathbf{r})\hat{\mathbf{A}}(\mathbf{r}) \tag{S12}$$

so called because of its appearance in the minimal coupling Hamiltonian. The elementary field-free current $\hat{\mathbf{j}}(\mathbf{r})$ and charge density $\hat{\sigma}(\mathbf{r})$ are defined as

$$\hat{\mathbf{j}}(\mathbf{r}) = \frac{1}{2i}\left(\hat{\psi}^\dagger(\mathbf{r})\nabla\hat{\psi}(\mathbf{r}) - (\nabla\hat{\psi}^\dagger(\mathbf{r}))\hat{\psi}(\mathbf{r})\right), \tag{S13}$$

$$\hat{\sigma}(\mathbf{r}) = \hat{\psi}^\dagger(\mathbf{r})\hat{\psi}(\mathbf{r}) \tag{S14}$$

where $\hat{\psi}^\dagger(\mathbf{r})$ and $\hat{\psi}(\mathbf{r})$ are the electron field creation and annihilation operators, which satisfy the Fermi anti-commutation relation

$$\{\hat{\psi}(\mathbf{r}), \hat{\psi}^\dagger(\mathbf{r}')\} = \delta(\mathbf{r} - \mathbf{r}'). \tag{S15}$$

We start with the minimal coupling Hamiltonian Eq. 1 (7, 8). Signals involving the $\hat{\mathbf{j}}(\mathbf{r}) \cdot \hat{\mathbf{A}}(\mathbf{r})$ term are accompanied by a factor $\mathbf{A}(\omega)(\omega - \hat{H})^{-1}$ where ω is an optical detuning frequency and so become negligible compared to the $\hat{\sigma}A^2$ term in the off-resonant limit while dominating the resonant response. In the off-resonant case, the light scattering signal is then solely related to the charge-density and the associated elastic scattering is known as diffraction (9, 10). The vector potential is written as a field mode expansion

$$\hat{\mathbf{A}}(\mathbf{r}) = \sum_{\mathbf{k}_j\lambda_j} \sqrt{\frac{2\pi}{\Omega\omega_j}}\left(\epsilon^{(\lambda_j)}(\mathbf{k}_j)\hat{a}_j e^{i\mathbf{k}_j\cdot\mathbf{r}} + \epsilon^{(\lambda_j)*}(\mathbf{k}_j)\hat{a}_j^\dagger e^{-i\mathbf{k}_j\cdot\mathbf{r}}\right) \tag{S16}$$

with $\hat{a}_j$ ($\hat{a}_j^{(\dagger)}$) the photon field boson annihilation (creation) operator for mode j, Ω the field quantization volume and $\epsilon^{(\lambda_j)}(\mathbf{k}_j)$ the polarization vector.

The photon scattering signal is defined as the expectation value of the time integrated, rate-of-change of photon number $\hat{N}_s = \hat{a}_s^\dagger\hat{a}_s$ in a selected signal mode s

$$S(\mathbf{k}_s) = \int \mathrm{d}t \left\langle \frac{\mathrm{d}\hat{N}_s}{\mathrm{d}t} \right\rangle. \tag{S17}$$

In a more rigorous account of light scattering signals, the detection process could be explicitly modeled, e.g., as a two-level detector coupled to the scattered electric field (11–13). One is then required to sum over emission directions and frequencies, with temporal and spectral selectivity being added only later by detector details. In diffraction experiments, the detected field mode s is initially in the vacuum state and we must sum over modes. We can thus separate the modes into two disjoint sets: field modes which are initially in the vacuum state and those corresponding to an external light pulse. We then have

$$\hat{\mathbf{A}}(\mathbf{r}) = \hat{\mathbf{A}}^{(\mathrm{v})}(\mathbf{r}) + \hat{\mathbf{A}}^{(\mathrm{p})}(\mathbf{r}) \tag{S18}$$

where the "v" superscript indicates the vacuum modes and the "p" indicates modes occupied by an incoming pulse. Later, we will make a semiclassical approximation and replace $\hat{\mathbf{A}}^{(\mathrm{p})}(\mathbf{r})$ by its expectation value. For now, our treatment will remain general and the pulse modes will be kept quantum-mechanical.

We start with the Heisenberg equation of motion for the photon number operator $\hat{N}_s = a^\dagger a$

$$\frac{\mathrm{d}\hat{N}_s}{\mathrm{d}t} = -i[\hat{N}_s, \hat{H}_{\mathrm{int}}] = i\int \mathrm{d}\mathbf{r}\left(\hat{\mathbf{j}}(\mathbf{r})\cdot[\hat{N}_s, \hat{\mathbf{A}}^{(\mathrm{v})}(\mathbf{r})] - \frac{1}{2}\hat{\sigma}(\mathbf{r})[\hat{N}_s, \hat{\mathbf{A}}^{(\mathrm{v})2}(\mathbf{r})] + 2\hat{\mathbf{A}}^{(\mathrm{p})}(\mathbf{r})\cdot[\hat{N}_s, \hat{\mathbf{A}}^{(\mathrm{v})}(\mathbf{r})]\right) \quad [S19]$$

where we have used the relations $[\hat{N}_s, \hat{\mathbf{A}}^{(\mathrm{p})}(\mathbf{r})] = 0 = [\hat{\mathbf{A}}^{(\mathrm{v})}(\mathbf{r}), \hat{\mathbf{A}}^{(\mathrm{p})}(\mathbf{r})]$. It is straightforward to calculate the commutators

$$[\hat{N}_s, \hat{\mathbf{A}}^{(\mathrm{v})}(\mathbf{r})] = \mathbf{A}_s^*(\mathbf{r})\hat{a}_s^\dagger - \mathrm{c.c.} \quad [S20]$$

$$[\hat{N}_s, \hat{\mathbf{A}}^{(\mathrm{v})2}(\mathbf{r})] = 2(\hat{a}_s^\dagger \mathbf{A}_s^* \cdot \hat{\mathbf{A}}^{(\mathrm{v})}(\mathbf{r}) - \mathrm{c.c.}). \quad [S21]$$

Here, $\mathbf{A}_s(\mathbf{r}) = \sqrt{\frac{2\pi}{\Omega\omega_s}}\epsilon^{(\lambda_s)}(\mathbf{k}_s)e^{i\mathbf{k}_s\cdot\mathbf{r}}$ (and complex conjugate). Inserting these commutators into Eq. S19 then gives

$$\dot{\hat{N}}_s = 2\Im\left[\int \mathrm{d}\mathbf{r}\left(\hat{\mathbf{j}}(\mathbf{r})\cdot\mathbf{A}_s(\mathbf{r})\hat{a}_s - \hat{\sigma}(\mathbf{r})(\hat{\mathbf{A}}^{(\mathrm{v})}(\mathbf{r})\cdot\mathbf{A}_s(\mathbf{r})\hat{a}_s + \hat{\mathbf{A}}^{(\mathrm{p})}(\mathbf{r})\cdot\mathbf{A}_s(\mathbf{r})\hat{a}_s)\right)\right] \quad [S22]$$

Defining the total electromagnetic current in the presence of the vector potential

$$\hat{\mathbf{J}}(\mathbf{r}) = -\frac{1}{2}\left[\hat{\psi}^\dagger(\mathbf{r})\mathbf{v}\hat{\psi}(\mathbf{r}) + (\mathbf{v}\hat{\psi}(\mathbf{r}))^\dagger\hat{\psi}(\mathbf{r})\right] = \hat{\mathbf{j}}(\mathbf{r}) - \hat{\sigma}(\mathbf{r})\hat{\mathbf{A}}(\mathbf{r}), \quad [S23]$$

where $\mathbf{v} = (-i\nabla + \hat{\mathbf{A}})$ is the velocity operator, we then have for the signal

$$S(\mathbf{k}_s) = -2\Im\left[\int \mathrm{d}t\mathrm{d}\mathbf{r}\langle\hat{a}_s^\dagger\mathbf{A}_s^*(\mathbf{r})\cdot\mathbf{J}(\mathbf{r})\rangle\right] \quad [S24]$$

where we have used $\Im[z] = -\Im[z^\dagger]$ to bring the expression to the conventional form in which the last interaction may be interpreted as an emission from the ket. Equation S24 is exact as we have made no approximations thus far. The time-dependence in this equation comes through the expectation value, which we evaluate in the interaction picture with respect to $\hat{H}_{\mathrm{int}}$ (Eq. 1):

$$\langle\hat{a}_s^\dagger\mathbf{A}_s^*(\mathbf{r})\cdot\mathbf{J}(\mathbf{r})\rangle = \mathrm{Tr}\left[\hat{a}_s^\dagger\mathbf{A}_s^*(\mathbf{r})\cdot\mathbf{J}(\mathbf{r})\mathcal{T}\; e^{-i\int_{-\infty}^{t} d\tau\hat{H}_{\mathrm{int}-}(\tau)}\right] \quad [S25]$$

Thus far, we have instead worked in the Heisenberg picture. The difference will be to add an explicit time-dependence to all material operators. The free evolution time-dependence for the fields will be absorbed into their coefficients $\mathbf{A}_j(\mathbf{r}) \mapsto \mathbf{A}_j(\mathbf{r},t) = \mathbf{A}_j(\mathbf{r})e^{-i\omega_j t}$. We note that a zeroth-order expansion of the expectation value in (S24) would vanish due to the $\langle 0_s|\hat{a}_s^\dagger$ factor. We thus require an additional order in $\hat{H}_{\mathrm{int}}$ which must act on the bra, to yield

$$S(\mathbf{k}_s) = 2\Re\left[\int \mathrm{d}t\mathrm{d}\mathbf{r}\mathrm{d}\mathbf{r}'\int_{-\infty}^{t}\langle\hat{\mathbf{J}}_{\mathrm{int}}(\mathbf{r}',t')\cdot\hat{\mathbf{A}}(\mathbf{r}',t')\hat{a}_s^\dagger\mathbf{A}_s^*(\mathbf{r},t)\cdot\mathbf{J}(\mathbf{r},t)\rangle\right]. \quad [S26]$$

This expression does not vanish even without further expansion of the propagator.We may thus obtain the lowest-order contribution to the photon scattering into mode s by tracing over that mode at this point. Using the commutators

$$[\hat{a}_s^\dagger, \hat{\mathbf{A}}(\mathbf{r})] = -\mathbf{A}_s(\mathbf{r}) \quad [S27]$$

$$[\hat{a}_s^\dagger, \hat{\mathbf{J}}_{\mathrm{int}}(\mathbf{r})] = \frac{1}{2}\hat{\sigma}(\mathbf{r})\mathbf{A}_s(\mathbf{r}), \quad [S28]$$

and taking the trace over mode s (using the fact that $\hat{a}_s|0\rangle_s = 0$), we obtain

$$S(\mathbf{k}_s) = 2\Re\left[\int \mathrm{d}t\mathrm{d}\mathbf{r}\mathrm{d}\mathbf{r}'\int_{-\infty}^{t}\mathrm{d}t'\langle\mathbf{A}_s(\mathbf{r}',t')\cdot\hat{\mathbf{J}}(\mathbf{r}',t')\hat{\mathbf{J}}(\mathbf{r},t)\cdot\mathbf{A}_s^*(\mathbf{r},t)\rangle\right]. \quad [S29]$$

The expectation value in the above expression excludes mode s (since it was already traced over) and it is not technically the same as those in previous expressions, we keep the notation $\langle\ldots\rangle$ rather than making the difference explicit. The dot products in Eq. S29 serve merely to pick out the projection of the current $\mathbf{J}$ along the vector potential $\mathbf{A}_s$. Equation S29 can also be recast in the symmetric form

$$S(\mathbf{k}_s) = \int \mathrm{d}t\mathrm{d}t'\mathrm{d}\mathbf{r}\mathrm{d}\mathbf{r}'\langle\mathbf{A}_s(\mathbf{r}',t')\cdot\hat{\mathbf{J}}(\mathbf{r}',t')\hat{\mathbf{J}}(\mathbf{r},t)\cdot\mathbf{A}_s^*(\mathbf{r},t)\rangle \quad [S30]$$

which further simplifies to

$$S(\mathbf{k}_s) = \frac{2\pi}{\Omega\omega_s}\int \mathrm{d}t\mathrm{d}t'\mathrm{d}\mathbf{r}\mathrm{d}\mathbf{r}'e^{-i\mathbf{k}_s\cdot(\mathbf{r}-\mathbf{r}')+i\omega_s(t-t')}\times\left[\epsilon^{(\lambda_s)*}(\hat{\mathbf{k}}_s)\cdot\langle\hat{\mathbf{J}}(\mathbf{r}',t')\hat{\mathbf{J}}(\mathbf{r},t)\rangle\cdot\epsilon^{(\lambda_s)*}(\hat{\mathbf{k}}_s)\right]. \quad [S31]$$

Multiplying by the density $\Omega/(2\pi)^3$ of states in $\mathbf{k}_s$ space and by the volume element of $\mathbf{k}_s$ space per solid angle per unit frequency

$$\frac{\mathrm{d}\mathbf{k}_s}{\mathrm{d}\Omega_s \mathrm{d}\omega_s} = \frac{\omega_s^2}{c^3} \tag{S32}$$

we obtain

$$S(\mathbf{k}_s) = \frac{\alpha^3 \omega_s}{4\pi^2} \left[\epsilon^{(\lambda_s)*}(\hat{\mathbf{k}}_s) \cdot \langle \hat{\mathbf{J}}(-\mathbf{k}_s, -\omega_s) \hat{\mathbf{J}}(\mathbf{k}_s, \omega_s) \rangle \cdot \epsilon^{(\lambda_s)*}(\hat{\mathbf{k}}_s) \right]. \tag{S33}$$

where we have employed the Fourier transform for compactness. In the main text, we will retain the form of an integral over time-dependent currents (see Eq. 2 of the main text) in order to better discuss ultrafast pump-probe scattering experiments in which the time-dependence is key. It should be noted that, in textbook derivations of scattering in the minimal coupling picture, the incoming field is frequently treated quantum mechanically as a plane wave. The resulting mode-quantization prefactor, once accounting for the incoming photon flux gives an additional factor of α/ω_p. The Thomson scattering cross section is then proportional to $\alpha^4 \omega_s/\omega_p$. In this manuscript and our previous work, we treat the incoming field in the semiclassical limit (i.e., as a large-amplitude coherent state) to allow a simple treatment of the X-ray temporal envelope. This method is more appropriate to consideration of ultrafast pump-probe diffraction rather than the more traditional static diffraction.

Inserting the definition of $\hat{\mathbf{J}}$ into Eq. S33 results in terms that contain only the electronic charge density $\hat{\sigma}$, only the electronic current density $\hat{j}$, and cross terms that contain both. The focus of this manuscript is the $\hat{\sigma}$-only terms which are responsible off-resonant scattering and thus diffraction signals. Since off-resonant scattering is often well-approximated as not changing the material state, time-dependent diffraction can be used to track changes in charge density, directly monitoring the motion of nuclei in the sample (14**?** –19) and single-molecule diffraction that would eliminate the necessity of crystallization with this technique has long been eagerly anticipated (20, 21).

As an aside, we also note that, as discussed briefly in the main text, a similar formalism applies to electron scattering (22–27). In that case, one can consider the process as populating a vacuum mode of the fermionic electron field rather than the photon field. Of course, the interaction Hamiltonian is completely different so the scattering will not be the same (e.g., in the independent atom approximation the form factors will be different).

Eigenstate Expansions of S_1 and S_2

In terms of the exact electronic+vibrational eigenstates, the time-dependence of of the charge density operators in Eqs. 6 and 7 of the main text becomes trivial and we have

$$S_1(\mathbf{q}, T) = N \int \mathrm{d}t |E_p(t-T)|^2 \sum_{IJK} \rho_{IJ} \hat{\sigma}_{JK}(-\mathbf{q}) \hat{\sigma}_{KI}(\mathbf{q}) e^{-i\omega_{IJ}t} \tag{S34}$$

$$S_2(\mathbf{q}, T) = F(\mathbf{q}) \int \mathrm{d}t |E_p(t-T)|^2 | \sum_{IJ} \rho_{IJ} e^{-i\omega_{IJ}t} \hat{\sigma}(\mathbf{q})|^2. \tag{S35}$$

We note that, due to the impulsive approximation that the ket and bra interactions with the X-ray field are simultaneous, there is no dependence on the frequency of the transition state K. In the case that particular transitions are to be observed, this is obviously not a good approximation and relaxing this assumption gives

$$\begin{aligned} S_1(\mathbf{q}, T) =& N \int \mathrm{d}t \mathrm{d}t' E_p(t-T) E_p^*(t'-T) \\ & \times \sum_{IJK} \rho_{IJ} \hat{\sigma}_{JK}(-\mathbf{q}) \hat{\sigma}_{KI}(\mathbf{q}) e^{-i(\omega_{IK}t - \omega_{KJ}t')}, \end{aligned} \tag{S36}$$

and

$$S_2(\mathbf{q}, T) = F(\mathbf{q}) \left| \int \mathrm{d}t E_p(t-T) \sum_{IJ} \rho_{IJ} e^{-i\omega_{IJ}t} \hat{\sigma}_{IJ}(\mathbf{q}) \right|^2 \tag{S37}$$

The Debye-Waller Factor

The effect of structural disorder in a crystal, e.g., due to phonons, is to attenuate the Bragg scattering (which originates from the average structure) and produce a diffuse scattering that, while still reaching its maximum value at the Bragg peaks, is present throughout broad regions of reciprocal space (28–30). This can be readily quantified with the Debye-Waller factor, which results from averaging the exponential in $F(\mathbf{q})$ over Gaussian spatial fluctuations of atomic positions and takes the form of

$$F_{\mathrm{DW}}(\mathbf{q}) = \langle e^{i\mathbf{q}\cdot\mathbf{u}_\alpha} \rangle_{\mathrm{T}}^2 = e^{-q^2 \langle u_\alpha^2 \rangle_{\mathrm{T}}/3} \tag{S38}$$

where $\mathbf{u}_\alpha$ is the displacement from equilibrium of molecule α and $\langle\dots\rangle_{\mathrm{T}}$ stands for a thermal average. The Debye-Waller factor is commonly used to describe the degradation of the Bragg pattern due to unavoidable small-amplitude disorder caused by phonons in real samples at finite temperature but it applies for any Gaussian disorder that can be treated exactly by the second-order cumulant expansion. By applying it for large fluctuations, we can interpolate between ordered and highly disordered samples. Note that the Debye-Waller factor does not represent simple broadening of the Bragg peaks (which conseves their intensity) as suggested by Kirkwood. It rather attenuates the Bragg peaks and introduces non-Bragg diffuse scattering (31).

Multi-Point Correlation Functions of the charge density

The two- and three-photon coincidence signals can be written so as to adjust the momentum transfer $\mathbf{q}$ to account for the material transition induced by the scattered X-ray pulse as (32)

$$\begin{aligned}S_{PC-2D}(\mathbf{k}_1,T_1,\mathbf{k}_2,T_2) =&|\omega_I\omega_{II}A_1(\omega_I)A_2(\omega_{II})|^2\\ &\times\int\Pi_i\mathrm{d}\mathbf{r}_i e^{-i\mathbf{q}_1\cdot(\mathbf{r}_1-\mathbf{r}_2)}e^{-i\mathbf{q}_2\cdot(\mathbf{r}_3-\mathbf{r}_4)}\\ &\times\langle\sigma^\dagger(\mathbf{r}_2,T_1+\mathbf{k}_I\cdot\mathbf{r}_2/c)\sigma^\dagger(\mathbf{r}_4,T_1+T_2+\mathbf{k}_{II}\cdot\mathbf{r}_4/c)\\ &\times\sigma(\mathbf{r}_3,T_1+T_2+\mathbf{k}_{II}\cdot\mathbf{r}_3/c)\sigma(\mathbf{r}_1,T_1+\mathbf{k}_I\cdot\mathbf{r}_1/c)\rangle\end{aligned}\tag{S39}$$

where $\Pi_i\mathrm{d}\mathbf{r}_i$ stands for the product over integration variables and

$$\begin{aligned}S_{PC-3D}(\mathbf{k}_1,T_1,\mathbf{k}_2,T_2,\mathbf{k}_3,T_3) = |\omega_I\omega_{II}\omega_{III}A_1(\omega_I)A_2(\omega_{II})A_3(\omega_{III})|^2\int\Pi_i\mathrm{d}\mathbf{r}_i e^{-i\mathbf{q}_1\cdot(\mathbf{r}_1-\mathbf{r}_2)}e^{-i\mathbf{q}_2\cdot(\mathbf{r}_3-\mathbf{r}_4)}e^{-i\mathbf{q}_2\cdot(\mathbf{r}_5-\mathbf{r}_6)}\\ \times\langle\sigma^\dagger(\mathbf{r}_2,T_1+\mathbf{k}_I\cdot\mathbf{r}_2/c)\sigma^\dagger(\mathbf{r}_4,T_1+T_2+\mathbf{k}_{II}\cdot\mathbf{r}_4/c)\sigma^\dagger(\mathbf{r}_6,T_1+T_2+T_3+\mathbf{k}_{III}\cdot\mathbf{r}_6/c)\\ \times\sigma(\mathbf{r}_5,T_1+T_2+T_3+\mathbf{k}_{III}\cdot\mathbf{r}_5/c)\sigma(\mathbf{r}_3,T_1+T_2+\mathbf{k}_{II}\cdot\mathbf{r}_3/c)\sigma(\mathbf{r}_1,T_1+\mathbf{k}_I\cdot\mathbf{r}_1/c)\rangle.\end{aligned}\tag{S40}$$

Diffraction of resonant pulses

In the paper, we have assumed that the last scattering event took place through the $\sigma\mathbf{A}^2$ coupling Hamiltonian. This is the common case in diffraction experiments whereby the scattered pulse is off-resonant with core transitions. On the other hand, resonant interactions are usually treated at the multipolar level and the spatial profile of the signal is then lost. In this appendix, we present diffraction signals obtained using resonant interactions. This forms a bridge between diffraction and spectroscopy.

Following the procedure of Appendix 2, we can derive the S_1 and S_2 signals for a resonant interaction with the s mode of the field.

$$S_1(\mathbf{k}_s) = \big(\frac{1}{2\epsilon_0\omega_s}\big)^2\sum_\alpha\Im\int\mathrm{d}t\mathrm{d}t' e^{-i\omega_s t'}e^{i\omega_s t}\langle\mathbf{j}_L(\mathbf{k}_s,t)\cdot\mathbf{j}_R^\dagger(-\mathbf{k}_s,t')\rangle\tag{S41}$$

$$S_2(\mathbf{k}_s) = \big(\frac{1}{2\epsilon_0\omega_s}\big)^2\sum_{\alpha\beta}\Im\int\mathrm{d}t\mathrm{d}t' e^{-i\omega_s t'}e^{i\omega_s t}e^{i\mathbf{k}_s(\mathbf{r}_\alpha-\mathbf{r}_\beta)}\times\langle\mathbf{j}_L(\mathbf{k}_s,t)\rangle\cdot\langle\mathbf{j}_R^\dagger(-\mathbf{k}_s,t')\rangle\tag{S42}$$

As an example, we consider four-wave mixing by expanding these signals to fourth order in $\mathbf{A}$ followed by a resonant scattering event:

$$\begin{aligned}S_1(\mathbf{k}_s) = \big(\frac{1}{2\epsilon_0\omega_s}\big)^2\sum_\alpha\Im\int(\Pi_i\mathrm{d}\mathbf{r}_i)(\Pi\mathrm{d}t_i)e^{-i\omega_s t'}e^{i\omega_s t}\langle\mathcal{T}\mathbf{j}_L(\mathbf{k}_s,t)\mathbf{j}_-(\mathbf{r}_3-\mathbf{r}_\alpha,t_3)\mathbf{j}_-(\mathbf{r}_2-\mathbf{r}_\alpha,t_2)\mathbf{j}_-(\mathbf{r}_1-\mathbf{r}_\alpha,t_1)\\ \times\mathbf{j}_R^\dagger(-k_s,t')\mathbf{j}_-(\mathbf{r}'_3-\mathbf{r}_\alpha,t'_3)\mathbf{j}_-(\mathbf{r}'_2-\mathbf{r}_\alpha,t'_2)\mathbf{j}_-(\mathbf{r}'_1-\mathbf{r}_\alpha,t'_1)\rangle\mathbf{A}(\mathbf{r}_3,t_3)\mathbf{A}(\mathbf{r}_2,t_2)\mathbf{A}(\mathbf{r}_1,t_1)\mathbf{A}(\mathbf{r}'_3,t'_3)\mathbf{A}(\mathbf{r}'_2,t'_2)\mathbf{A}(\mathbf{r}'_1,t'_1)\end{aligned}\tag{S43}$$

$$\begin{aligned}S_2(\mathbf{k}_s) = \big(\frac{1}{2\epsilon_0\omega_s}\big)^2\sum_{\alpha\beta}\Im\int(\Pi_i\mathrm{d}\mathbf{r}_i)(\Pi\mathrm{d}t_i)e^{-i\omega_s t'}e^{i\omega_s t}e^{i\mathbf{k}_s(\mathbf{r}_\alpha-\mathbf{r}_\beta)}\langle\mathbf{j}_L(\mathbf{k}_s,t)\mathbf{j}_-(\mathbf{r}_3-\mathbf{r}_\alpha,t_3)\mathbf{j}_-(\mathbf{r}_2-\mathbf{r}_\alpha,t_2)\mathbf{j}_-(\mathbf{r}_1-\mathbf{r}_\alpha,t_1)\rangle\\ \times\mathbf{A}(\mathbf{r}_3,t_3)\mathbf{A}(\mathbf{r}_2,t_2)\mathbf{A}(\mathbf{r}_1,t_1)\langle\mathbf{j}_R^\dagger(-\mathbf{k}_s,t')\mathbf{j}_-(\mathbf{r}'_3-\mathbf{r}_\beta,t'_3)\mathbf{j}_-(\mathbf{r}'_2-\mathbf{r}_\beta,t'_2)\mathbf{j}_-(\mathbf{r}'_1-\mathbf{r}_\beta,t'_1)\rangle\mathbf{A}(\mathbf{r}'_3,t'_3)\mathbf{A}(\mathbf{r}'_2,t'_2)\mathbf{A}(\mathbf{r}'_1,t'_1)\end{aligned}\tag{S44}$$

Where the "-" denotes the commutation superoperator associated with a Hilbert space operator O, $O_-X\equiv[O,X]$.

If the field spatial envelope does not vary appreciably over the current charge density, the field can be written as $\mathbf{A}(\mathbf{r}_3,t_3)=\mathbf{A}(t_3)e^{\pm i\mathbf{k}_3\cdot\mathbf{r}_3}$.

$$\begin{aligned}S_1(\mathbf{k}_s)=\frac{1}{\epsilon_0\omega_s}\int\Pi\mathrm{d}t_i\,\langle\mathcal{T}\mathbf{j}_L(\mathbf{k}_s,t)\mathbf{j}_-(\mp\mathbf{k}_3,t_3)\mathbf{j}_-(\mp\mathbf{k}_2,t_2)\mathbf{j}_-(\mp\mathbf{k}_1,t_1)\\ \times\mathbf{j}_R^\dagger(-\mathbf{k}_s,t')\mathbf{j}_-(\pm\mathbf{k}_3,t_3')\mathbf{j}_-(\pm\mathbf{k}_2,t_2')\mathbf{j}_-(\pm\mathbf{k}_1,t_1')\rangle\\ \times\mathbf{A}(t_3)\mathbf{A}(t_2)\mathbf{A}(t_1)\mathbf{A}(t_3')\mathbf{A}(t_2')\mathbf{A}(t_1')\end{aligned}\tag{S45}$$

$$\begin{aligned}S_2(\mathbf{k}_s)=&2\Im F(\mathbf{k}_s\pm\mathbf{k}_3\pm\mathbf{k}_2\pm\mathbf{k}_1)\\ &\times\left|\frac{1}{2\epsilon_0\omega_s}\int\Pi\mathrm{d}t_i\langle\langle 1|\mathbf{j}_L(\mathbf{k}_s,t)\mathbf{j}_-(\mp\mathbf{k}_3,t_3)\mathbf{j}_-(\mp\mathbf{k}_2,t_2)\mathbf{j}_-(\mp\mathbf{k}_1,t_1)|\rho\rangle\rangle\mathbf{A}(t_3)\mathbf{A}(t_2)\mathbf{A}(t_1)\right|^2\end{aligned}\tag{S46}$$

The F function, Eq. 6, is strongly peaked near $\mathbf{k}_s\pm\mathbf{k}_3\pm\mathbf{k}_2\pm\mathbf{k}_1=0$ and we then recover the direction of emission of resonant signals in the dipole approximation. If the field does vary over the current density, we have to stick with Eqs. D3 and D4. These signals contain all the information of standard resonant spectroscopy with additional structural information through the $\mathbf{k}_s$ variation. In the main text, we started from $\mathbf{q}$ resolved signals and added a time resolution to it. Diffraction schemes thus give access to the $(\mathbf{q},\mathbf{r})$ couple and the (ω,t) variables are accessible through careful preparation of the matter. In this appendix, we started with resonant spectroscopic signals that naturally contain (ω,t) information and added structural information $(\mathbf{q},\mathbf{r})$ by considering a regime in which the multipolar approximation does not apply. It is worth noting that this approach is experimentally challenging in small objects since the spatial field envelope has to vary appreciably over the current density distribution. Nanofields are good candidates to achieve an interesting spatial resolution (33). As mentioned briefly in the main text, such current-dependent expressions can, under certain conditions (such as when the material acts twice with each of a well-separated pair of pump and probe pulses), be recast in terms of effective polarizabilities. This approach is analogous to that of resonant Raman (34).

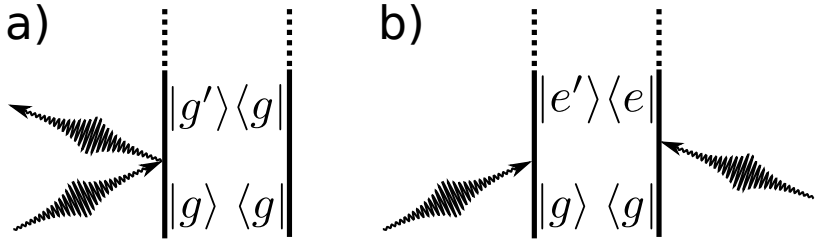

Fig. S1. Preparation of the non-stationary state with a UV pump-pulse. Shown are two types of the initial state preparation which are schematically represented by the grey boxes in the lower parts of the loop diagrams in Figs. 1-2. (a) A Raman process creates a nuclear oscillating wave packet in the electronic ground state. (b) An optical absorption prepares a nuclear wave packet in an electronic excited state.

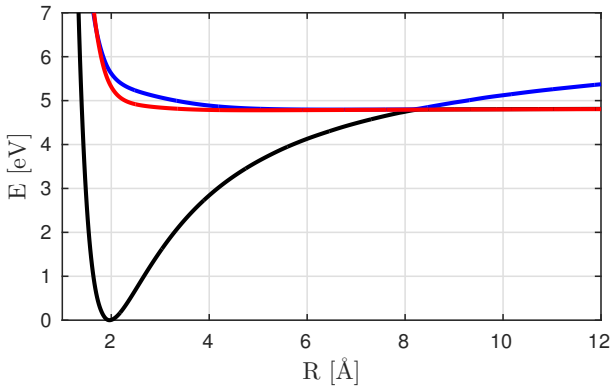

Fig. S2. Relevant adiabatic potential energy surfaces of NaF (ionic $X\,^1\Sigma$ black, covalent $A\,^1\Sigma$, blue, $^1\Pi$, red).

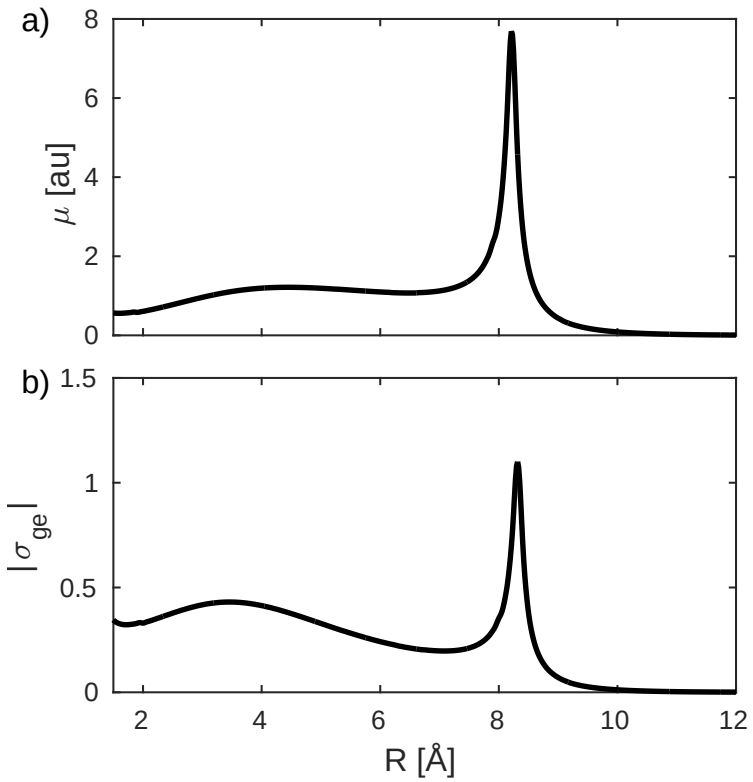

Fig. S3. Transition dipole moment μ_{ge} between the X and A states of NaF (a) and magnitude of the transition density σ_{ge} (b).

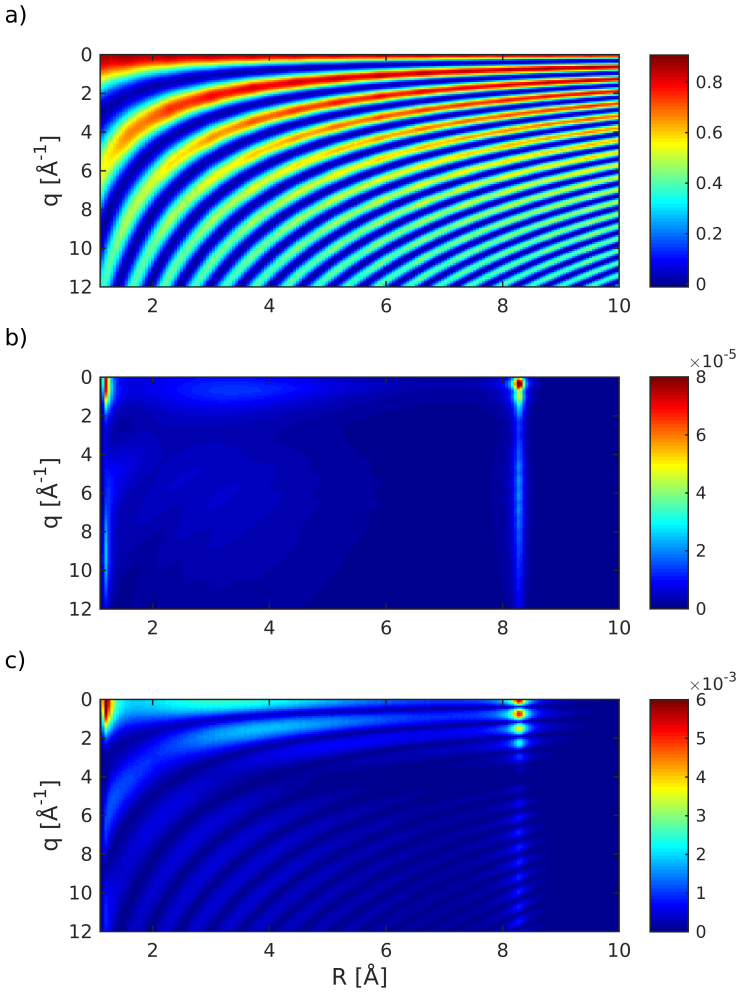

Fig. S4. Selected charge density operator matrix elements in the nuclear subspace of NaF (obtained using Eq. S1: (a) $\hat{\sigma}^2_{ee}(\mathbf{q}, R)$, (b) $\hat{\sigma}^2_{ge}(\mathbf{q}, R)$, (c) $|\hat{\sigma}^\dagger_{ee}(\mathbf{q}, R)\hat{\sigma}_{ge}(\mathbf{q}, R)|$.

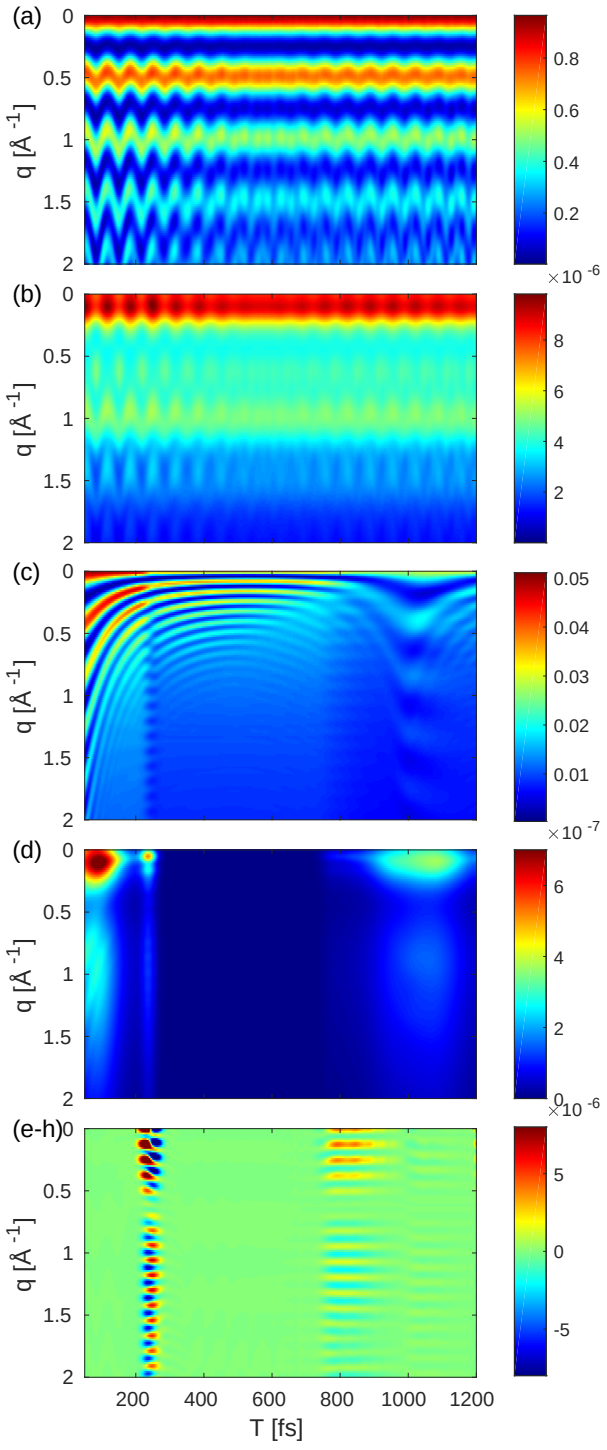

Fig. S5. Time-dependent gas-phase diffraction signal of NaF ($S_1(q,T)$, Fig. 6) broken down into its contributions. The labeling of the sub figures is identical with the labeling of terms in Eq. 11: (a) elastic contribution from the ground state; (b) and (d) inelastic contribution from the ground and excited state respectively; (c) elastic contribution from the excited state; (e-h) Sum over inelastic contributions scattering off the electronic coherence. All intensities are normalized with respect to the total signal.

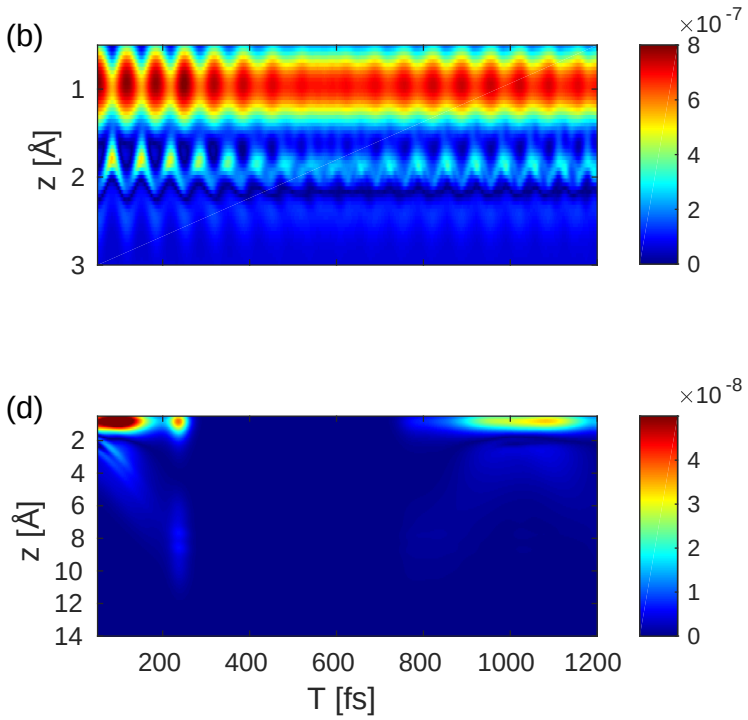

Fig. S6. Contributions to the real space signal $S_1(z,T)$ (inverse Fourier transform of $S_1(q_z,T)$) from the transition charge densities (terms (b) and (d)). The labeling of the sub figures is identical with the labeling of terms in Eq. 11.

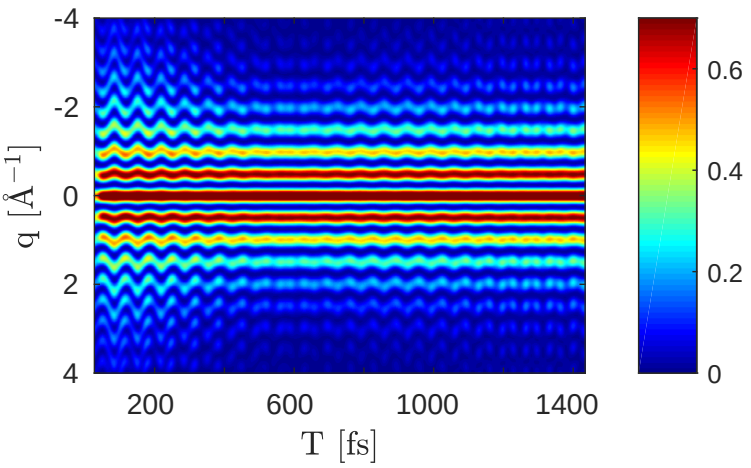

Fig. S7. Two-molecule contribution for NaF according to Eq. 18, considering only the ground state. The diffraction pattern is domintated by the electronic ground state. Signal intensities are given relative to the total S_2 signal.

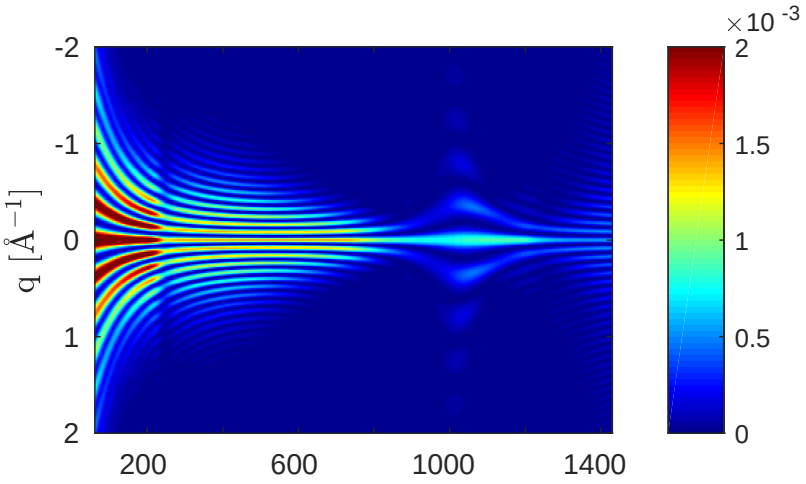

Fig. S8. Two-molecule contribution for NaF according to Eq. 18, considering only the excited-state wave packet. Signal intensities are given relative to total S_2 signal.

References

1. Werner HJ, Knowles PJ, Knizia G, Manby FR, Schütz M (2015) Molpro, version 2015.1, a package of ab initio programs. see http://www.molpro.net.
2. Douglas M, Kroll NM (1974) Quantum electrodynamical corrections to the fine structure of helium. *Ann. Phys.-New York* 82(1):155.
3. Hess BA (1986) Relativistic electronic-structure calculations employing a two-component no-pair formalism with external-field projection operators. *Phys. Rev. A* 33(6):3742.
4. Domcke W, Yarkony DR, Köppel H (2011) *Conical Intersections*. (WORLD SCIENTIFIC) Vol. 17.
5. Hofmann A, de Vivie-Riedle R (2001) Adiabatic approach for ultrafast quantum dynamics mediated by simultaneously active conical intersections. *Chem. Phys. Lett.* 346(3-4):299–304.
6. Ezer HT, Kosloff R (1984) An accurate and efficient scheme for propagating the time dependent schrödinger equation. *J. Chem. Phys.* 81(9):3967–3971.
7. Power E, Thirunamachandran T (1978) On the nature of the hamiltonian for the interaction of radiation with atoms and molecules: $(e/mc)\mathbf{p}\cdot\mathbf{A} - \mu\cdot\mathbf{E}$, and all that. *Am. J. Phys.* 46(4):370–378.
8. Cohen-Tannoudji C, Dupont-Roc J, Grynberg G, Thickstun P (1992) *Atom-photon interactions: basic processes and applications*. (Wiley Online Library).
9. Guinier A (1994) *X-ray diffraction: in crystals, imperfect crystals, and amorphous bodies*. (Courier Dover Publications).
10. Als-Nielsen J, McMorrow D (2011) *Elements of modern X-ray physics*. (Wiley, Hoboken).
11. Glauber RJ (2007) *The Quantum Theory of Optical Coherence*. (Wiley-VCH Verlag GmbH & Co. KGaA).
12. Mandel L, Wolf E (1995) *Optical coherence and quantum optics*. (Cambridge university press).
13. Bennett K, Biggs JD, Zhang Y, Dorfman KE, Mukamel S (2014) Time-, frequency-, and wavevector-resolved x-ray diffraction from single molecules. *J. Chem. Phys.* 140(20):204311.
14. Siwick BJ, Dwyer JR, Jordan RE, Miller RD (2003) An atomic-level view of melting using femtosecond electron diffraction. *Science* 302(5649):1382–1385.
15. Ihee H, et al. (2005) Ultrafast x-ray diffraction of transient molecular structures in solution. *Science* 309(5738):1223–1227.
16. Cammarata M, et al. (2008) Tracking the structural dynamics of proteins in solution using time-resolved wide-angle x-ray scattering. *Nat. Methods* 5(10):881–886.
17. Siders CW, et al. (1999) Detection of nonthermal melting by ultrafast X-ray diffraction. *Science* 286(5443):1340–1342.
18. Larsson J, Falcone RW, , et al. (1998) Ultrafast structural changes measured by time-resolved X-ray diffraction. *Appl. Phys. A Mater. Sci. Process.* 66(6):587–591.
19. Coppens P, Vorontsov II, Graber T, Gembicky M, Kovalevsky AY (2005) The structure of short-lived excited states of molecular complexes by time-resolved x-ray diffraction. *Acta Crystallogr. A* 61(2):162–172.
20. Hajdu J (2000) Single-molecule X-ray diffraction. *Curr. Opin. Struct. Biol.* 10(5):569–573.
21. Stevens RC (2000) High-throughput protein crystallization. *Curr. Opin. Struct. Biol.* 10(5):558–563.
22. Baum P, Zewail AH (2009) 4D attosecond imaging with free electrons: Diffraction methods and potential applications. *Chem. Phys.* 366(1-3):2–8.
23. Zewail AH (2010) Four-dimensional electron microscopy. *Science* 328(5975):187–193.
24. Schäfer S, Liang W, Zewail AH (2010) Structural dynamics and transient electric-field effects in ultrafast electron diffraction from surfaces. *Chem. Phys. Lett.* 493(1):11–18.
25. Miller RD (2014) Femtosecond crystallography with ultrabright electrons and x-rays: capturing chemistry in action. *Science* 343(6175):1108–1116.
26. van der Veen RM, Penfold TJ, Zewail AH (2015) Ultrafast core-loss spectroscopy in four-dimensional electron microscopy. *Struct. Dynam.* 2(2):024302.
27. Yang J, et al. (2016) Diffractive imaging of coherent nuclear motion in isolated molecules. *Phys. Rev. Lett.* 117(15):153002.
28. Welberry T, Weber T (2016) One hundred years of diffuse scattering. *Crystallogr. Rev.* 22(1):2–78.
29. Welberry TR (2004) *Diffuse x-ray scattering and models of disorder*. (Oxford University Press on Demand) Vol. 16.
30. Debye P (1913) Interferenz von röntgenstrahlen und wärmebewegung. *Annalen der Physik* 348(1):49–92.
31. Kaufman B, Lipkin HJ (1962) Momentum transfer to atoms bound in a crystal. *Ann. Phys. New York* 18(2):294–309.
32. Biggs JD, Bennett K, Zhang Y, Mukamel S (2014) Multidimensional scattering of attosecond x-ray pulses detected by photon-coincidence. *J. Phys. B At. Mol. Opt.* 47(12):124037.
33. Novotny L, Hecht B (2012) *Principles of nano-optics*. (Cambridge university press).
34. Biggs JD, Zhang Y, Healion D, Mukamel S (2012) Two-dimensional stimulated resonance Raman spectroscopy of molecules with broadband X-ray pulses. *J. Chem. Phys.* 136:174117.